Published in final edited form as:
Cancer Res. 2014 December 15; 74(24): 7229–7238. doi:10.1158/0008-5472.CAN-14-1809.

Bioengineered implantable scaffolds as a tool to study stromal-derived factors in metastatic cancer models

Francesca Bersani[1,5], **Jungwoo Lee**[2,5], **Min Yu**[1,3], **Robert Morris**[1], **Rushil Desai**[1], **Sridhar Ramaswamy**[1], **Mehmet Toner**[2], **Daniel A. Haber**[1,3,*], and **Biju Parekkadan**[2,4,*]

[1]Cancer Center and Department of Medicine, Massachusetts General Hospital, Harvard Medical School, Charlestown, MA 02129

[2]Center for Engineering in Medicine and Surgical Services, Massachusetts General Hospital, Harvard Medical School and the Shriners Hospitals for Children, Boston, MA 02129

[3]Howard Hughes Medical Institute, Chevy Chase, MD 20815

[4]Harvard Stem Cell Institute, Boston, MA 02114

Abstract

Modeling the hematogenous spread of cancer cells to distant organs poses one of the greatest challenges in the study of human metastasis. Both tumor-cell intrinsic properties as well as interactions with reactive stromal cells contribute to this process, but identification of relevant stromal signals has been hampered by the lack of models allowing characterization of the metastatic niche. Here we describe an implantable bioengineered scaffold, amenable to *in vivo* imaging, *ex vivo* manipulation and serial transplantation for the continuous study of human metastasis in mice. Orthotopic or systemic inoculation of tagged human cancer cells into the mouse leads to the release of circulating tumor cells (CTCs) into the vasculature, which seed the scaffold, initiating a metastatic tumor focus. Mouse stromal cells can be readily recovered and profiled, revealing differential expression of cytokines, such as IL-1β, from tumor-bearing versus unseeded scaffolds. Finally, this platform can be used to test the effect of drugs on suppressing initiation of metastatic lesions. This generalizable model to study cancer metastasis may thus identify key stromal-derived factors with important implications for basic and translational cancer research.

Keywords

Bioengineered scaffold; metastasis; stroma; microenvironment; IL-1β

[*]Corresponding Authors: Daniel A. Haber, Massachusetts General Hospital Cancer Center, 149 13 St, Charlestown, MA 02129. Phone: 617-726-7805; Fax: 617-724-6919; haber@helix.mgh.harvard.edu. Biju Parekkadan, Massachusetts General Hospital Center for Engineering in Medicine, 51 Blossom St, Boston, MA 02114. Phone: 617-371-4874; Fax: 617-371-4951; biju_parekkadan@hms.harvard.edu.
[5]These authors contributed equally to this work

Disclosure of Potential Conflicts of Interest
The authors declare no competing financial interests.

INTRODUCTION

Despite significant advances in targeted therapies against cancer, metastatic disease remains incurable (1). Paget's 'seed and soil' hypothesis suggests that a receptive pre-metastatic microenvironment must evolve in order for tumor cells to engraft and proliferate at secondary sites (2, 3). Tumor cell-derived factors that enhance or direct metastasis to specific organs have been described (4–6). In contrast, proteins secreted by stromal cells within a metastatic niche are less readily identified, in part because of the difficulty in isolating and characterizing such cells even in mouse models. Such studies are particularly challenging in prostate and breast cancer, which metastasize to bone, a site that is not easily accessible for sampling.

A number of stromal-derived survival factors have been proposed based on *in vitro* coculture experiments, although most remain to be validated *in vivo* (7, 8). No robust mouse models exist to test for metastasis-enhancing stromal-derived factors on a scale that would allow identification of novel pathways and testing of potential therapeutic suppressors of critical tumor/stromal interactions. Bioengineered scaffolds have been previously employed for the study of primary tumors (9) and, for bone metastasis in particular, engineered bone marrow-like structures have recently been described in the context of hematopoietic reconstitution (10–12), but their application to generating and studying blood-borne metastasis have not been extensively explored. Here we present a bioengineered bone marrow-modeling scaffold, which can be implanted subcutaneously, monitored *in situ* through live imaging, and either serially transplanted *in vivo* or resected for detailed cellular and molecular analysis. Hematogenous seeding of the scaffold by orthotopically and systemically introduced tumor cells recapitulates the initiation of metastasis and allows molecular characterization of mouse-derived metastasis-associated stromal cells. As a functional validation of this method, we identify IL-1β as a stromal-secreted cytokine that enhances the initiation of metastasis in two different cancer models, and whose suppression can be achieved through systemic administration of a receptor antagonist. Our data demonstrate the efficacy of a metastasis-capturing device in uncovering stromal signals and evaluating the effect of their modulation *in vivo*, thus enabling broad applications in the study of cancer metastasis.

MATERIALS AND METHODS

All chemicals and supplies were purchased from Sigma Aldrich or Fisher Scientific unless otherwise stated. *In vivo* studies were performed in accordance with an animal protocol approved by the MGH Subcommittee on Research Animal Care.

Scaffold design

Scaffold design and bone marrow stromal cell seeding density were based on our previous studies that optimized these parameters (11). Specifically, we used a polyacrylamide hydrogel composed of 30%(w/w) acrylamide (monomer) and 5%(w/w) bis-acrylamide (crosslinker). Mechanical property of hydrogel scaffold measured by dynamic storage modulus was 18.3 ± 6.8 kPa. Cavity and junction diameters were about 250 μm and 65 μm, respectively. Half a million human bone marrow stromal cells were seeded per scaffold.

Pore dimension and porosity of scaffolds are comparable to the marrow tissue formed within trabecular bones, which consist of 300–900 μm cavities. Mechanical stiffness of hydrogel scaffolds is approximately 50-time higher than reported central marrow stiffness (13). Although decreasing the polymer content of the hydrogel matrix could further reduce mechanical stiffness, it cannot support open porous 3D structure during cell seeding and after subdermal implantation, which would in turn cause poor tissue development. Technical details about scaffold fabrication and 3D culture of primary human bone marrow stromal cells are provided in Supplementary Materials and Methods.

Cancer cell cultures and generation of Luc-GFP stable cell lines

PC-3 cells (ATCC) were cultured in F-12K Medium (ATCC), while DU-145 (ATCC) and MDA-231 #1833 (a kind gift by J. Massagué) were grown in DMEM (Gibco/Life Technologies), both supplemented with 10% FBS and 1% Pen/Strep (Gibco/Life Technologies). All cell lines were obtained in 2011 and immediately expanded and frozen at early passages. When thawed for experimental use, they were never passaged for more than four months in culture. ATCC-derived cell lines were authenticated by the cell bank via short tandem repeat profiling. MDA-231 #1833 where validated in our laboratory for KRAS and BRAF mutation by Sanger sequencing. All cells were tested for mycoplasma contamination giving negative results. Stable Luc-GFP cell lines were generated using high titer lentivirus (Lenti Luc-GFP) as previously described (14).

Drugs

For *in vitro* treatments, recombinant human IL-1β (PeproTech) and IL-1Ra (Anakinra, Sobi) were resuspended as 100 μg/ml stocks in DMSO and used at a concentration of 100 ng/ml.

For *in vivo* experiments, IL-1Ra (Anakinra, Sobi) stock solution (100 mg/0.67 ml) was freshly diluted in PBS at the moment of use and administered daily by IP injection at a concentration of 25 mg/kg.

In vitro invasion and proliferation assays

Invasiveness and proliferation of PC-3 cells were assessed according to standard procedures with slight modifications. Details are provided in Supplementary Materials and Methods.

Subdermal scaffold implant, explant and transplant

Six to eight week-old male NOD/SCID/IL2γ^{null} (NSG) mice (Jackson Laboratory) were used for xenograft studies. The dorsal side of mice was shaved under isofluorane anesthesia. BMSC-coated scaffolds were washed with PBS (x3 times). After wiping the skin with alcohol swap, a ~4 mm incision was made to create a subcutaneous pocket, a scaffold was carefully inserted using forceps and the incision was closed with surgical staples (Roboz). Four scaffolds were implanted in each mouse. On the last day of the study, mice were scarified and implanted scaffolds were carefully removed. For serial transplant, explanted scaffolds were subdermally re-implanted as described above.

Xenograft mouse models, bioluminescence (BLI) imaging and *in vivo* IL-1Ra treatment

Four BMSC-coated scaffolds were subcutaneously implanted in the back of each mouse as previously described. Four weeks later, orthotopic prostate tumors were generated by injecting 1×10^6 PC-3 or DU-145 cells into the dorsal prostatic gland of NSG mice in a volume of 20 μl (1:1 ratio of PBS and Matrigel Basement Membrane Matrix, BD Biosciences). Similarly, experimental breast cancer metastases were generated by tail vein injection of 1×10^6 MDA-231 #1833 cells in the same strain of immunocompromised mice. Animals were imaged weekly 5 min after IP injection of 150 μl RediJect D-Luciferin Ultra Bioluminescent Substrate (Caliper Life Sciences) using an IVIS Lumina II platform (Caliper Life Sciences) with constant settings throughout the entire experiment. Four or eight weeks later (breast and prostate cancer model, respectively), mice were sacrificed and scaffolds were explanted for either culture, histological analysis or serial transplantation into syngeneic tumor-free mice. Bone and visceral metastases were confirmed on dissected organs immediately after necropsy based on BLI and GFP fluorescence. Bioluminescence in recipient mice was monitored weekly for up to eight more weeks as described above. For drug treatment, PC-3 tumor-bearing mice were randomized based on primary tumor size and treated daily by IP injection of 25 mg/kg IL-1Ra or PBS vehicle (4 mice per group) for two weeks starting six weeks after establishment of the primary tumor, followed by scaffold transplantation as above. The investigator performing live imaging of transplanted mice (experiment readout) was blinded to the group allocation.

CTC capture and enumeration

Before scaffold transplant, PC-3 tumor-bearing mice were anesthetized to perform cardiocentesis through the intercostal muscle of the left chest and approximately 1 ml of blood was drawn into a syringe primed with 100 μl of PBS with 10mM EDTA pH 7.4 (Gibco). CTCs were isolated by depleting the normal blood cell component using a microfluidic platform (^{neg}CTC-iChip) as previously described (15). Cells were collected, spun down onto a microscope slide and fixed with 4% PFA. Samples were then permeabilized with 1% NP40 in PBS, blocked with 2% goat serum, and immunostained with chicken anti-GFP primary antibody (Abcam, ab13970) followed by donkey anti-chicken Dylight 488 secondary antibody (Jackson ImmunoResearch, 703-486-155). Slides were imaged under 10x magnification using the BioView Ltd automated imaging system, and hand-validated to enumerate CTCs.

Ex vivo imaging and culture of explanted scaffolds

Explanted scaffolds recovered from tumor-bearing mice were cultured for up to four weeks in F-12K Medium (ATCC) or DMEM (Gibco/Life Technologies) + 10% FBS + 1% Pen/Strep (Gibco/Life Technologies) and imaged weekly with an IVIS Lumina II platform (Caliper Life Sciences) after incubation in a 1:200 dilution of RediJect D-Luciferin Ultra Bioluminescent Substrate (Caliper Life Sciences) for 15 min at 37°C.

Recovery of live cells from scaffolds, FACS isolation and gene expression profiling

Seeded (met+) and unseeded (met−) scaffolds were minced with a scalpel and the cellular component was digested with collagenase IV in 1X HBSS (Gibco/Life Technologies) for 45

min at 37°C and filtered through a 70 μm cell strainer. After 1 min incubation in ACK lysing buffer (Gibco/Life Technologies), cells were washed and resuspended in PBS-2% FBS solution. Cells were stained with anti-mouse CD45-Biotin (eBioscience, 13-0451-81, clone 30-F11) and anti-mouse CD31-Biotin (eBioscience, 13-0311-81, clone 390) followed by Streptavidin-APC incubation (eBioscience, 17-4317-82). To avoid unwanted spillover from the very bright GFP signal into channels excited by the same laser and in order to reach maximum sorting stringency of pure stromal cells, we opted for a combination of CD45 and CD31 in the same channel (APC) using a different excitation laser. Cell sorting was performed on a four laser FACSAria II (BD Biosciences) based on endogenous GFP and antibody-linked APC fluorescence. DAPI staining was used for dead cell exclusion. Collected GFP−/CD45−/CD31− cells were lysed in Trizol followed by standard RNA isolation. Equivalent amounts of RNA (50 ng) were reverse transcribed using RT^2 First Strand Kit and cDNA was pre-amplified with RT^2 PreAMP Primer Mix (SABiosciences/Qiagen) according to the manufacturer's instructions. Each sample was loaded on a Mouse Tumor Metastasis RT^2 Profiler PCR Array (SABiosciences/Qiagen) for real-time PCR-based quantitation of gene expression on an ABI/PRISM 7500 platform (Applied Biosystems/Life Technologies). Quality control, normalization against the arithmetic mean of four different housekeeping genes, data analysis and generation of scatter plots were done with the RT^2 Profiler PCR Array Data Analysis v3.5 software (SABiosciences/Qiagen). Briefly, normalized expression of each gene between the two groups (met+ and met−) was plotted against one another. The central line in the plots in Figure 4A indicates unchanged gene expression. Boundaries (fold regulation cut-off) were set at 5-fold change. Gene-wise ANOVA followed by T-test between PC-3 met+, MDA-231 #1833 met+ and met− qPCR samples was performed to identify differentially expressed genes. Correction for multiple hypotheses was carried out using the Benjamini-Hochberg procedure and genes with FDR<0.1 were considered significant. For standard flow cytometry analysis (BD FACSCalibur), CD45−/CD31− cells sorted from scaffolds four weeks after subdermal implant were stained with APC-anti-human HLA-ABC (BD Pharmingen, 555555) or Biotin-anti-mouse CD44 (BD Pharmingen, 553132, clone IM7) followed by Streptavidin-APC (eBioscience, 17-4317-82).

Histological analysis

For immunohistochemistry, PC-3 cells and tissue sections (see below) were fixed with 4% paraformaldehyde, permeabilized with 0.1% Triton-X solution and then blocked with 10% normal goat serum and 1% bovine serum albumin solution diluted in PBS. Samples were serially incubated with rat anti-mouse CD31 (BD Pharmingen, 55027), mouse anti-human Cytokeratin 7&8 (BD Biosciences, 349205) or mouse anti-human Vimentin antibody (DAKO, 7165), followed by biotinylated goat anti-rat or goat anti-mouse IgG (Vecta Lab, BA-9400 and BA-9200) and ABC solution (Vecta Lab). Signal was visualized by applying DAB substrate (Vecta Lab).

Explanted scaffolds were embedded in optical cutting temperature compound and snap-frozen with dry ice-chilled 2-methylbutane. Frozen scaffold blocks were cut to 10–30 μm thickness and stored at −80°C until use. For hematoxylin/eosin, Giemsa, Trichrome and Periodic Acid-Schiff stainings, frozen tissue sections were fixed with 10% buffered formalin

solution and stained following the vendor's protocol (American Master Tech). For immunofluorescence stainings, frozen tissue sections were fixed with ice-cold acetone, blocked with 10% normal goat serum and 1% bovine serum albumin diluted in PBS. Slides were incubated with rat anti-mouse CD31 (BD Pharmingen, 55027), mouse anti-human Vimentin antibody (DAKO, 7165) or rabbit anti-human/mouse-IL-1β (Abcam, ab9722), followed by goat anti-rat IgG Alexa Fluor 594 (A11007), goat anti-mouse IgG Alexa Fluor 488 (A11029) or goat anti-rabbit IgG Alexa Fluor 680 (A21109; Invitrogen/Life Technologies). Finally, VectaShield mounting medium with DAPI was applied and slides were imaged under confocal (Leica SP5) and fluorescence (Zeiss 200) microscopes.

Scanning electron microscope (SEM) imaging

For scanning electron microscope imaging, *in vitro* cell-cultured and explanted scaffolds were fixed with 2% glutaradehyde, serially dehydrated with 20, 50, 70, 90, 95 and 100% ethanol solution, and further dried using a lyophilizer overnight. A thin platinum/gold film was deposited on the samples using a sputter coating machine (208HR, Cressington) and then samples were imaged under FESEM Ultra55 (Zeiss).

Analysis of IL-1β expression in primary tumors

We looked at the effect of grade/Gleason score on IL-1β expression in previously published datasets for prostate (16) and breast (17) cancer. In order to determine the relationship between IL-1β expression and grade/Gleason score, we collected log2 median centered intensity data and grade/Gleason categorical data from the Oncomine website (https://www.oncomine.org). With respect to the prostate cancer dataset a T-test was used to calculate the significance of the IL-1β expression change between 12 Gleason score 6 samples and 15 Gleason score 9 samples. Similarly, we used a T-test to calculate the significance of the IL-1β expression change between 19 grade I tumor and 69 grade III breast tumor samples. Statistics were calculated using R (http://www.r-project.org).

Meta-analysis of IL-1β expression between primary and metastatic tumors

A meta-analysis comparing IL-1β expression between metastatic and primary tumor samples was performed using data from two prostate (18, 19) and one breast (20) published datasets. We selected metastatic samples with higher IL-1β expression compared to the average IL-1β level of the primary samples (or paired primary in the case of (20)) within each experiment. Using this criterion we retained 8 unpaired (18), 11 unpaired (19) and 4 paired (20) sets of samples. The meta-analysis was performed using an in-house R script.

Statistics

Unless otherwise stated, *P* values were calculated based on a 2-tailed Student's *t* test. All sets of data met normal distribution. As an exception, a non-parametric Wilcoxon signed-rank test was applied to calculate the *P* value of the difference between the two cohorts of mice in the IL-1Ra drug experiment, where values were not following a parametric model. Values of $P<0.05$ were considered significant. All error bars represent standard deviation (SD) of three or more replicates, as indicated in each figure. The sample size of each experiment is specified in figures and legends.

RESULTS

Bioengineered scaffolds recapitulate metastasis-receptive microenvironments

We adapted a bioengineered surrogate to mimic the 3D microenvironment of bone marrow (BM) (11, 21–24) to study blood-borne metastases in epithelial cancers. The marrow-like structure, which enhances engraftment by hematopoietic elements and leukemia cell lines, made it an attractive model to study prostate and breast cancer metastases, which have tropism for bone (25). Hydrogel scaffolds were synthesized with the microarchitecture of bone marrow sinusoids through a pattern of repeating honeycombs, matching mechanical properties of soft trabecular spongy bone (Fig. 1A and Supplementary Fig. S1A). These scaffolds were conjugated with type I collagen and they effectively supported the adhesion and proliferation of introduced primary human bone marrow stromal cells (BMSCs). The BMSCs secreted growth factors, chemokines, and ECM that are concentrated within the hydrogel (Fig. 1B). Compared with non-cellularized scaffolds, BMSC coating led to increased invasion by human cancer cells, as measured in a modified Boyden chamber assay (Fig. 1C and Supplementary Fig. S1B). The seeding and proliferation of luciferase- and GFP-tagged (Luc-GFP) cells was also significantly enhanced by BMSC-coating of scaffolds in a cell density-dependent manner (Fig. 1D and Supplementary Fig. S1C).

When subcutaneously implanted on the back of immunocompromised (NSG) mice, BMSC-coated scaffolds progressively lost their human stromal cell constituent, as shown by *in vivo* imaging analysis of tagged stromal cells, as well as by loss of staining of the retrieved devices for cells bearing human HLA markers (Supplementary Fig. S2A–C). Within four weeks from implantation, human BMSC cells were fully replaced by endogenous mouse stromal cells (Fig. 1E and Supplementary Fig. S2C,D). At this time point, the majority (89.2%) of CD45−/CD31− mouse cells within the scaffold were scored positive for CD44 (Supplementary Fig. S2C), a marker enriched in mesenchymal cells, which plays an active role as a homing receptor and interacts with bone-specific ligands such as osteopontin (26–28). In addition, Masson’s trichrome staining revealed abundant presence of connective tissue (Fig. 1E), which makes this platform ideal to study microenvironmental changes at the stromal cell level.

We previously reported that the transient colonization by human BMSC serves to initiate the recruitment of murine hematopoietic precursors to the device (11), which is then sustained by mouse cells. Although we have not tested the sub-lineage differentiation ability of hematopoietic cells following recruitment to implanted scaffolds, we previously demonstrated active homing of endogenous mouse Lin−/Sca1+/c-kit+ progenitors as well as engraftment capacity for human CD34 cells (11).

Taken together, while the model that we established does not precisely recapitulate the bone marrow environment, it mimics some of its main physical and cellular characteristics and provides an effective platform to enable capture and analysis of newly established metastases in a model organism.

Implantable microenvironments can capture CTCs and support their engraftment

We developed an orthotopic tumor model, in which Luc-GFP-tagged cancer cells can be used for *in vivo* tracking of both the primary tumor and the metastatic deposits derived from hematogenous seeding of the implanted scaffolds (Fig. 1F). For these experiments, we implanted four BMSC-functionalized scaffolds on the back of each recipient NSG mouse, allowing them to become coated with mouse-derived stromal cells and vasculature. Four weeks later, 1×10^6 Luc-GFP PC-3 human prostate cancer cells were injected directly into the prostate, and mice were monitored using bioluminescence imaging (BLI) as they demonstrated a progressive increase in primary tumor burden (Fig. 2A and Supplementary Fig. S3A). PC-3 cells were chosen for their proven ability to generate circulating tumor cells (CTCs) in the blood of mice bearing orthotopic xenografts in the prostate (data not shown). Animals were sacrificed at two months, at which time primary prostate tumors weighted approximately 400 mg. CTCs were readily detectable in blood samples (range: 13–44 cells/ml/mouse) using a microfluidic capture platform (CTC-iChip) (15) (Fig. 2B). At the same time, *ex vivo* analysis of scaffolds using BLI revealed tumor cell-derived signal in 12/97 scaffolds (~12%; average met+ scaffolds/mouse: 0.58; range: 0–4) (Fig. 2C). In the 13 mice analyzed, the number of CTCs was correlated with the fraction of luciferase-positive scaffolds (R^2=0.97224), consistent with the presumed hematogenous seeding of the scaffolds (Fig. 2D). This finding highlights the ability of the scaffold to efficiently recruit tumor cells from circulation *in vivo*. PC-3 cells that had metastasized to the scaffolds were clearly identified by immunohistochemical staining using their characteristic markers, human Vimentin and Cytokeratin (Fig. 2E and Supplementary Fig. S4). Further culturing of individual explanted scaffolds *in vitro* for up to a month, yielded additional luciferase signal, with 14/40 (35%) becoming positive as rare tumor cells that had initially seeded the scaffolds *in vivo* were allowed to further proliferate in culture (Fig. 2F).

As control, we tested the efficiency of tumor cell seeding *in vivo* by other cancer cell types (Supplementary Fig. S3B,C). Poorly metastatic DU-145 prostate cancer cells (29) failed to engraft in the scaffold (0/10 scaffolds), despite generating sizable primary tumors in the prostate. In contrast, the highly aggressive MDA-231 #1833 breast cancer cell subline, which has been selected for enhanced tropism to bone (4), generated luciferase positive signal from 13/24 scaffolds (~54%), which all turned positive following one month in culture *ex vivo* (Supplementary Fig. S5).

Serial transplantation of CTC-harboring microenvironments allows cellular and molecular characterization of metastasis *in vivo*

The rapid expansion of primary prostate tumors in mice following orthotopic inoculation necessitated removal of the scaffolds before they are fully mature, as noted by the fact that some explanted devices turn luciferase-positive following *ex vivo* culture. To enable more complete monitoring of metastatic microenvironments as they evolve *in vivo*, we established a transplantation assay, whereby scaffolds are transplanted from tumor-bearing mice into naïve recipient mice (Fig. 3A). The specific biophysical characteristics of the scaffold allow successful transplants by minimizing time and manipulation of the pre-metastatic microenvironment formed *in vivo*, and recipient mice can then be imaged for an additional two months, without interference from a large primary tumor (Fig. 3B,C). Indeed, 26/68

scaffolds (~38%) were scored as met+ using this *in vivo* imaging end point, matching the frequency obtained after *ex vivo* culture (Fig. 2F). Tumor cell colonization of the devices was consistent with observation of visceral metastases in primary tumor-bearing mice. Of note, with this serial transplantation assay, none of the transplanted scaffolds from mice harboring DU-145 primary tumors (negative control) and all of those from mice with MDA-231 #1833 tumors (positive control) were scored positive by *in vivo* imaging at two months (Supplementary Fig. S6A–C). Serial transplantation of scaffolds allowed us to capture within each device the full evolution of metastasis, from initial extravasation and seeding of a single CTC to colonization and ECM degradation (Fig. 3D). Thus, integration of transplantable scaffolds with live imaging in orthotopic mouse tumor models may enable detailed characterization of the formation and progression of the metastatic niche *in vivo*.

Coexistence of tumor-infiltrated (met+) and tumor-free (met−) scaffolds within the same animal prompted us to explore differences in their microenvironment at the molecular level. Live cells were recovered from paired met+ and met− scaffolds, derived from 3 independent tumor-bearing mice. Distinct cell populations from matched met+ and met− scaffolds were stained for various cell surface markers and quantified by flow cytometry (Fig. 3E,F and Supplementary Fig. S6D,E). Consistent with a prior study showing direct competition between prostate cancer cells and hematopoietic stem cells in the bone marrow niche (30), we found that the hematopoietic/endothelial compartment (GFP−/mCD45+/mCD31+) was reduced in the presence of metastatic prostate cancer cells (GFP+) (Fig. 3F). This effect was even more marked for the highly invasive MDA-231 #1833 breast cancer cells (Supplementary Fig. S6E). In contrast, the relative number of stromal cells was not affected by tumor burden.

To further characterize the stromal compartment of tumor-infiltrated scaffolds, we compared RNA expression profiles from FACS sorted stromal cells derived from either met− or met+ scaffolds from the same tumor-bearing mouse, interrogating a pre-designed qPCR Array including 85 metastasis-related genes (Supplementary Table S1). Among the most commonly upregulated genes from met+ stromal cells (>5 fold change), we identified the cytokine IL–1β (Fig. 4A), matrix metalloproteinases (*Mmp-13*, *Mmp-10* and *Mmp-9)* that are known contributors to the pre-metastatic niche, as well as the angiogenesis-related tyrosine kinase *Flt-4*, the pro-metastatic gene *Etv-4* and the *Mcam* adhesion molecule. Among these, IL–1β was the most differentially induced gene in the PC-3 prostate cancer model (~3,600 fold; $P<0.005$; FDR<0.02) and it was also upregulated (~21 fold; $P<0.02$; FDR<0.05) in the MDA-231 breast cancer model (Fig. 4A). Immunohistochemical staining of met+ scaffolds confirmed that IL-1β expression was almost exclusively derived from stromal cells, rather cancer cells (Fig. 4B).

Implantable microenvironments provide an *in vivo* platform to identify relevant stromal-derived factors in cancer metastasis models

The expression of IL-1β by human cancers is well documented, although the source of its production may be variable. The cytokine may be derived from malignant cells themselves, from stromal cells in response to factors secreted by cancer cells (31), or as part of the inflammatory response that accompanies tumor growth (32). IL-1β overexpression itself is

associated with increased MMP expression, invasiveness, angiogenesis and tumor-mediated immune suppression (33–35). To confirm the physiological significance of IL-1β expression as it relates to metastatic propensity, we tested a well annotated prostate cancer dataset (16). Expression of IL-1β by primary prostate tumors was positively correlated with their Gleason score, a well defined histological marker of invasiveness and metastatic recurrence risk (Fig. 4C). A similar correlation between histological grade and IL-1β expression was evident in our analysis of a large breast cancer dataset (17) (Fig. 4C). Furthermore, a meta-analysis of multiple available datasets (18–20) showed significant upregulation of IL-1β in both prostate and breast cancer metastases, compared with primary tumors (Fig. 4D). All available datasets are based on gene expression profiling of bulk primary or metastatic tumors, thus containing a mixed population of cancer cells and stromal cells. The elevation in IL-1β expression may therefore be even greater in a pure stromal cell population. These clinical correlations are consistent with previous reports of IL-1 expression in several invasive tumor types (33, 36, 37).

To test the reliability of our new scaffold-based method to identify relevant metastatic stromal components and verify the functional significance of stromal cell IL-1β expression, we treated prostate tumor-bearing mice carrying subcutaneous scaffolds with either an FDA-approved IL-1 receptor antagonist (IL-1Ra) or vehicle control (4 mice and 16 scaffolds per test group). Mice were treated daily for two weeks, beginning six weeks after orthotopic inoculation of prostate cancer cells. At the time of IL-1Ra treatment, primary tumors were readily detectable by BLI *in vivo* imaging, but the scaffolds were not yet scored positive. After two weeks of treatment, scaffolds were transplanted into naïve recipient mice, which were monitored for the development of metastases without further treatment for an additional two months (Fig. 4E). IL-1Ra-treated mice showed a 50% reduction in the number of met+ scaffolds: 3/16 (18.7%) met+ scaffolds in treated mice versus 6/16 (37.5%) scaffolds in controls ($P<0.005$). The positive scaffolds derived from IL-1Ra-treated mice also had a dramatic reduction in luciferase signal intensity (Fig. 4F). Since tumor-bearing mice were treated only for a limited time before transplantation of scaffolds into naïve mice, it is likely that IL-1β contributes to the early recruitment of CTCs to the scaffold rather than supporting tumor cell proliferation after engraftment. Consistent with this model, IL-1Ra had no effect on PC-3 cell proliferation *in vitro* (Supplementary Fig. S7A). PC-3 met+ scaffolds derived from untreated mice also showed no growth advantage or growth suppression, following *ex vivo* culture in the presence of either recombinant IL-1β or IL-1Ra (Supplementary Fig. S7B).

DISCUSSION

The importance of the microenvironment in metastatic progression is well established, but our understanding of the precise contribution of specific factors and cell populations, which have been extensively studied at the primary tumor level (38, 39), is limited at secondary sites. Given the technical hurdles incidental to recovering and studying the stromal compartment of the metastatic niche *in vivo*, we aimed to develop an experimental method to test whether a bioengineered scaffold could be used to dissect the cellular components of a metastatic lesion. As increasing numbers of therapeutic agents are developed to target the tumor-supporting stroma within bone metastases (40), there is a need for controllable

models that mimic physiological tumor/stromal interactions *in vivo*, extending beyond standard available *in vitro* coculture experimental conditions (7, 8). Metastases to distant organs are infrequent in mouse tumor models (41), and these are rarely accessible for detailed molecular analysis. The biocompatible scaffold described here circumvents these technical limitations based on its high efficiency engraftment by blood-borne CTCs, as well as its susceptibility to serial *in vivo* passaging and monitoring and *ex vivo* cellular and molecular analysis. This versatile platform to capture viable metastasis-competent CTCs and analyze their interactions with host stromal cells builds on previous approaches (42, 43), enabling study of the evolution of the metastatic niche at different stages of tumor progression. For instance, we show that explanting tumor-seeded scaffolds at different time points allows characterization of changes within the stromal compartment that may allow the establishment of a metastatic focus.

In providing a proof of concept of the ability of our platform to uncover relevant stromal signals involved in CTC recruitment and initiation of metastatic lesions, we confirmed the pivotal role for the IL-1β cytokine in promoting tumor cell engraftment. In our experiments, IL-1β expression was detected within stromal cells of tumor-bearing but not tumor-free scaffolds, and its role in enhancing metastatic seeding of the bioengineered scaffold by prostate PC-3 cancer cells was supported by the effectiveness of a receptor antagonist administered systemically. Our observations are consistent with a recent report of increased bone metastases following intracardiac injection of IL-1β-transduced prostate cancer cells in the mouse (37). In these experiments, knockdown of endogenous IL-1β within injected tumor cells had no effect in reducing the frequency of metastatic lesions, supporting our observation that stromal cell expression may be the more physiological source of this cytokine, rather than tumor cells. Of note, additional stromal-derived factors were evident in our analysis of scaffolds bearing either prostate or breast cancer colonization, some of which overlap, suggesting that our platform may have broad utility in characterizing tumor/stromal interactions across multiple tumor types. Among the differentially expressed genes identified in metastatic stroma, some, such as MMPs, chemokines (*Ccl7*) and chemokine receptors (*Cxcr2*, *Cxcr4*) are likely involved in the formation of a receptive microenvironment, whereas others, such as tyrosine kinase receptors (*Flt-4*) and transcription factors (*Etv-4*) possibly favor the active growth of a secondary tumor mass. Both the engraftment and the growth-promoting aspects, although difficult to distinguish, contribute to the homing and generation of bone metastasis and can be interrogated using the transplantable scaffold described in this study. As exemplified by the consequences of suppressing IL-1β in the PC-3 cell model, identification of key factors implicated in tumor/stromal crosstalk may lead to potential therapeutic intervention.

Taken together, this integrated approach, involving implantation of bioengineered devices into mouse tumor models followed by cellular and molecular characterization of colonizing cell populations, offers a powerful tool to study the metastatic microenvironment, dissect molecular changes within different components of the metastatic niche and model tumor/stromal interactions *in vivo*.

Supplementary Material

Refer to Web version on PubMed Central for supplementary material.

Acknowledgments

Grant Support

This work was supported in part by NIH Grants R01EB012521 (B.P.), K01DK087770 (B.P.), K99CA163671 (J.L.), R01CA129933 (D.A.H., F.B.); the Shriners Hospitals for Children (J.L., B.P.); the National Foundation for Cancer Research (D.A.H.), and the Howard Hughes Medical Institute (D.A.H.).

We are grateful to S. M. Rothenberg for help in developing the mouse models, to R. Murray for technical support in BMSC culture and *in vitro* characterization and to R. Mylvaganam from the MGH Flow Cytometry Core and M. Waring from the Ragon Institute for cell sorting. We also thank R. Taulli and all lab members for helpful discussions.

References

1. Coghlin C, Murray GI. Current and emerging concepts in tumour metastasis. J Pathol. 2010; 222:1–15. [PubMed: 20681009]
2. Psaila B, Lyden D. The metastatic niche: adapting the foreign soil. Nat Rev Cancer. 2009; 9:285–93. [PubMed: 19308068]
3. Fidler IJ. The pathogenesis of cancer metastasis: the ‘seed and soil’ hypothesis revisited. Nat Rev Cancer. 2003; 3:453–8. [PubMed: 12778135]
4. Kang Y, Siegel PM, Shu W, Drobnjak M, Kakonen SM, Cordon-Cardo C, et al. A multigenic program mediating breast cancer metastasis to bone. Cancer Cell. 2003; 3:537–49. [PubMed: 12842083]
5. Minn AJ, Gupta GP, Siegel PM, Bos PD, Shu W, Giri DD, et al. Genes that mediate breast cancer metastasis to lung. Nature. 2005; 436:518–24. [PubMed: 16049480]
6. Minn AJ, Kang Y, Serganova I, Gupta GP, Giri DD, Doubrovin M, et al. Distinct organ-specific metastatic potential of individual breast cancer cells and primary tumors. J Clin Invest. 2005; 115:44–55. [PubMed: 15630443]
7. Coulson-Thomas VJ, Gesteira TF, Coulson-Thomas YM, Vicente CM, Tersariol IL, Nader HB, et al. Fibroblast and prostate tumor cell cross-talk: fibroblast differentiation, TGF-beta, and extracellular matrix down-regulation. Exp Cell Res. 2010; 316:3207–26. [PubMed: 20727350]
8. Lescarbeau RM, Seib FP, Prewitz M, Werner C, Kaplan DL. In vitro model of metastasis to bone marrow mediates prostate cancer castration resistant growth through paracrine and extracellular matrix factors. PLoS One. 2012; 7:e40372. [PubMed: 22870197]
9. Villasante A, Marturano-Kruik A, Vunjak-Novakovic G. Bioengineered human tumor within a bone niche. Biomaterials. 2014; 35:5785–94. [PubMed: 24746967]
10. Torisawa YS, Spina CS, Mammoto T, Mammoto A, Weaver JC, Tat T, et al. Bone marrow-on-a-chip replicates hematopoietic niche physiology in vitro. Nat Methods. 2014
11. Lee J, Li M, Milwid J, Dunham J, Vinegoni C, Gorbatov R, et al. Implantable microenvironments to attract hematopoietic stem/cancer cells. Proc Natl Acad Sci U S A. 2012; 109:19638–43. [PubMed: 23150542]
12. Scotti C, Piccinini E, Takizawa H, Todorov A, Bourgine P, Papadimitropoulos A, et al. Engineering of a functional bone organ through endochondral ossification. Proc Natl Acad Sci U S A. 2013; 110:3997–4002. [PubMed: 23401508]
13. Shin JW, Swift J, Ivanovska I, Spinler KR, Buxboim A, Discher DE. Mechanobiology of bone marrow stem cells: from myosin-II forces to compliance of matrix and nucleus in cell forms and fates. Differentiation. 2013; 86:77–86. [PubMed: 23790394]
14. Lee J, Wang JB, Bersani F, Parekkadan B. Capture and printing of fixed stromal cell membranes for bioactive display on PDMS surfaces. Langmuir. 2013; 29:10611–6. [PubMed: 23927769]

15. Ozkumur E, Shah AM, Ciciliano JC, Emmink BL, Miyamoto DT, Brachtel E, et al. Inertial focusing for tumor antigen-dependent and -independent sorting of rare circulating tumor cells. Sci Transl Med. 2013; 5:179ra47.
16. Vanaja DK, Cheville JC, Iturria SJ, Young CY. Transcriptional silencing of zinc finger protein 185 identified by expression profiling is associated with prostate cancer progression. Cancer Res. 2003; 63:3877–82. [PubMed: 12873976]
17. Gluck S, Ross JS, Royce M, McKenna EF Jr, Perou CM, Avisar E, et al. TP53 genomics predict higher clinical and pathologic tumor response in operable early-stage breast cancer treated with docetaxel-capecitabine +/− trastuzumab. Breast Cancer Res Treat. 2012; 132:781–91. [PubMed: 21373875]
18. Taylor BS, Schultz N, Hieronymus H, Gopalan A, Xiao Y, Carver BS, et al. Integrative genomic profiling of human prostate cancer. Cancer Cell. 2010; 18:11–22. [PubMed: 20579941]
19. Chandran UR, Ma C, Dhir R, Bisceglia M, Lyons-Weiler M, Liang W, et al. Gene expression profiles of prostate cancer reveal involvement of multiple molecular pathways in the metastatic process. BMC Cancer. 2007; 7:64. [PubMed: 17430594]
20. Vecchi M, Confalonieri S, Nuciforo P, Vigano MA, Capra M, Bianchi M, et al. Breast cancer metastases are molecularly distinct from their primary tumors. Oncogene. 2008; 27:2148–58. [PubMed: 17952122]
21. Kotov NA, Liu Y, Wang S, Cumming C, Eghtedari M, Vargas G, et al. Inverted colloidal crystals as three-dimensional cell scaffolds. Langmuir. 2004; 20:7887–92. [PubMed: 15350047]
22. Lee J, Shanbhag S, Kotov N. Inverted colloidal crystals as three-dimensional microenvironments for cellular co-cultures. J Mater Chem. 2006; 16:3558–64.
23. Nichols JE, Cortiella J, Lee J, Niles JA, Cuddihy M, Wang S, et al. In vitro analog of human bone marrow from 3D scaffolds with biomimetic inverted colloidal crystal geometry. Biomaterials. 2009; 30:1071–9. [PubMed: 19042018]
24. Lee J, Kotov NA. Notch ligand presenting acellular 3D microenvironments for ex vivo human hematopoietic stem-cell culture made by layer-by-layer assembly. Small. 2009; 5:1008–13. [PubMed: 19334013]
25. Suva LJ, Washam C, Nicholas RW, Griffin RJ. Bone metastasis: mechanisms and therapeutic opportunities. Nat Rev Endocrinol. 2011; 7:208–18. [PubMed: 21200394]
26. Pittenger MF, Mackay AM, Beck SC, Jaiswal RK, Douglas R, Mosca JD, et al. Multilineage potential of adult human mesenchymal stem cells. Science. 1999; 284:143–7. [PubMed: 10102814]
27. Sackstein R, Merzaban JS, Cain DW, Dagia NM, Spencer JA, Lin CP, et al. Ex vivo glycan engineering of CD44 programs human multipotent mesenchymal stromal cell trafficking to bone. Nat Med. 2008; 14:181–7. [PubMed: 18193058]
28. Weber GF, Ashkar S, Glimcher MJ, Cantor H. Receptor-ligand interaction between CD44 and osteopontin (Eta-1). Science. 1996; 271:509–12. [PubMed: 8560266]
29. Connolly JM, Rose DP. Angiogenesis in two human prostate cancer cell lines with differing metastatic potential when growing as solid tumors in nude mice. J Urol. 1998; 160:932–6. [PubMed: 9720590]
30. Shiozawa Y, Pedersen EA, Havens AM, Jung Y, Mishra A, Joseph J, et al. Human prostate cancer metastases target the hematopoietic stem cell niche to establish footholds in mouse bone marrow. J Clin Invest. 2011; 121:1298–312. [PubMed: 21436587]
31. Schulze J, Weber K, Baranowsky A, Streichert T, Lange T, Spiro AS, et al. p65-Dependent production of interleukin-1beta by osteolytic prostate cancer cells causes an induction of chemokine expression in osteoblasts. Cancer Lett. 2012; 317:106–13. [PubMed: 22108531]
32. Korkaya H, Liu S, Wicha MS. Regulation of cancer stem cells by cytokine networks: attacking cancer's inflammatory roots. Clin Cancer Res. 2011; 17:6125–9. [PubMed: 21685479]
33. Lewis AM, Varghese S, Xu H, Alexander HR. Interleukin-1 and cancer progression: the emerging role of interleukin-1 receptor antagonist as a novel therapeutic agent in cancer treatment. J Transl Med. 2006; 4:48. [PubMed: 17096856]
34. Apte RN, Voronov E. Is interleukin-1 a good or bad 'guy' in tumor immunobiology and immunotherapy? Immunol Rev. 2008; 222:222–41. [PubMed: 18364005]

35. Spano D, Zollo M. Tumor microenvironment: a main actor in the metastasis process. Clin Exp Metastasis. 2012; 29:381–95. [PubMed: 22322279]

36. Soria G, Ofri-Shahak M, Haas I, Yaal-Hahoshen N, Leider-Trejo L, Leibovich-Rivkin T, et al. Inflammatory mediators in breast cancer: coordinated expression of TNFalpha & IL-1beta with CCL2 & CCL5 and effects on epithelial-to-mesenchymal transition. BMC Cancer. 2011; 11:130. [PubMed: 21486440]

37. Liu Q, Russell MR, Shahriari K, Jernigan DL, Lioni MI, Garcia FU, et al. Interleukin-1beta promotes skeletal colonization and progression of metastatic prostate cancer cells with neuroendocrine features. Cancer Res. 2013; 73:3297–305. [PubMed: 23536554]

38. Bissell MJ, Hines WC. Why don't we get more cancer? A proposed role of the microenvironment in restraining cancer progression. Nat Med. 2011; 17:320–9. [PubMed: 21383745]

39. Kidd S, Spaeth E, Watson K, Burks J, Lu H, Klopp A, et al. Origins of the tumor microenvironment: quantitative assessment of adipose-derived and bone marrow-derived stroma. PLoS One. 2012; 7:e30563. [PubMed: 22363446]

40. Saylor PJ, Lee RJ, Smith MR. Emerging therapies to prevent skeletal morbidity in men with prostate cancer. J Clin Oncol. 2011; 29:3705–14. [PubMed: 21860001]

41. Khanna C, Hunter K. Modeling metastasis in vivo. Carcinogenesis. 2005; 26:513–23. [PubMed: 15358632]

42. Moreau JE, Anderson K, Mauney JR, Nguyen T, Kaplan DL, Rosenblatt M. Tissue-engineered bone serves as a target for metastasis of human breast cancer in a mouse model. Cancer Res. 2007; 67:10304–8. [PubMed: 17974972]

43. Holzapfel BM, Wagner F, Loessner D, Holzapfel NP, Thibaudeau L, Crawford R, et al. Species-specific homing mechanisms of human prostate cancer metastasis in tissue engineered bone. Biomaterials. 2014; 35:4108–15. [PubMed: 24534484]

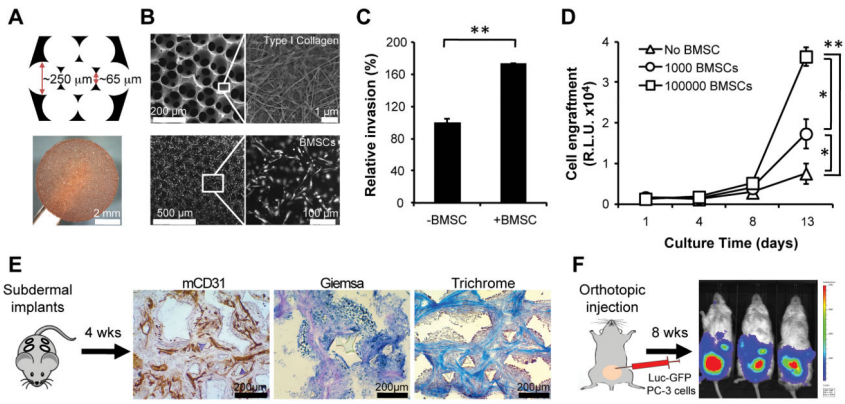

Figure 1.

Bone marrow-mimicking scaffolds promote invasion and growth of PC-3 prostate tumor cells *in vitro* and generate a marrow-like microenvironment *in vivo*. A, schematic (top) and image (bottom) of marrow-mimicking 3D porous hydrogel scaffold. B, scanning electron microscope (SEM) images of type I collagen-coated scaffolds (top) and primary human BMSC culture in a 3D scaffold (bottom). C, transwell-based PC-3 cell invasion assay in presence of BMSC-coated/uncoated scaffolds. Cell invasion in absence of BMSC was set at 100% (n=3). D, longitudinal monitoring of Luc-GFP PC-3 cell growth on BMSC-coated/uncoated scaffolds via tumor-specific bioluminescent activity (R.L.U., relative luciferase unit; n=6). Bars represent SD. *P<0.02, **P<0.005. E, mouse CD31, Giemsa and Trichrome stainings of scaffolds 4 weeks after subcutaneous implantation into NSG mice. F, representative BLI image of prostate tumor-bearing mice 8 weeks after orthotopic injection of Luc-GFP PC-3 cells.

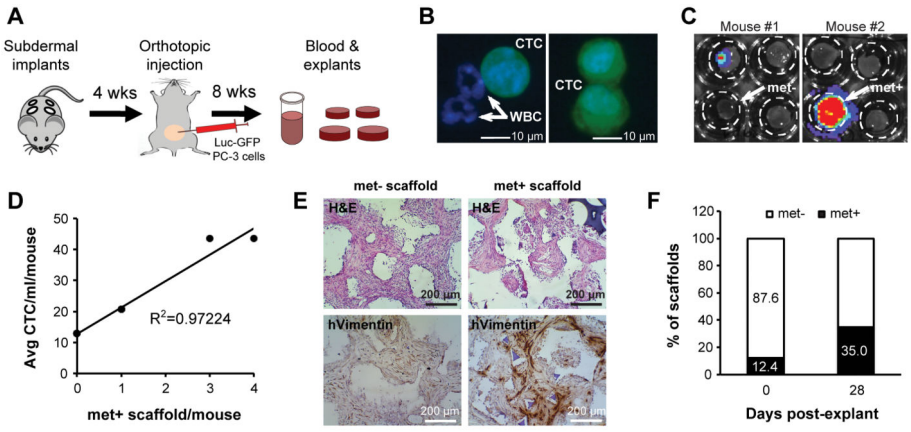

Figure 2.

Implanted scaffolds capture circulating tumor cells and sustain metastatic engraftment *ex vivo*. A, schematic of experimental procedure. B, representative images of circulating tumor cells (CTCs; GFP+ cells) captured by microfluidic CTC-iChip. White blood cells (GFP−) are indicated by arrows. C, bioluminescence imaging (BLI) of explanted scaffolds confirmed CTC engraftment in some of the scaffolds. D, whole blood from 13 animals was pooled into three separate groups depending on the number of luciferase-positive scaffolds/mouse, either 0 (6 mice), 1 (5 mice) or >1 (2 mice) and run on CTC-iChips. The number of met+ scaffold/mouse was then plotted against the average number of CTC/ml/mouse showing linear correlation. E, histological analysis of met− and met+ scaffolds by human-specific Vimentin. F, after 4 weeks of *ex vivo* culture, 35% of scaffolds exhibited positive BLI signal (*n*=40).

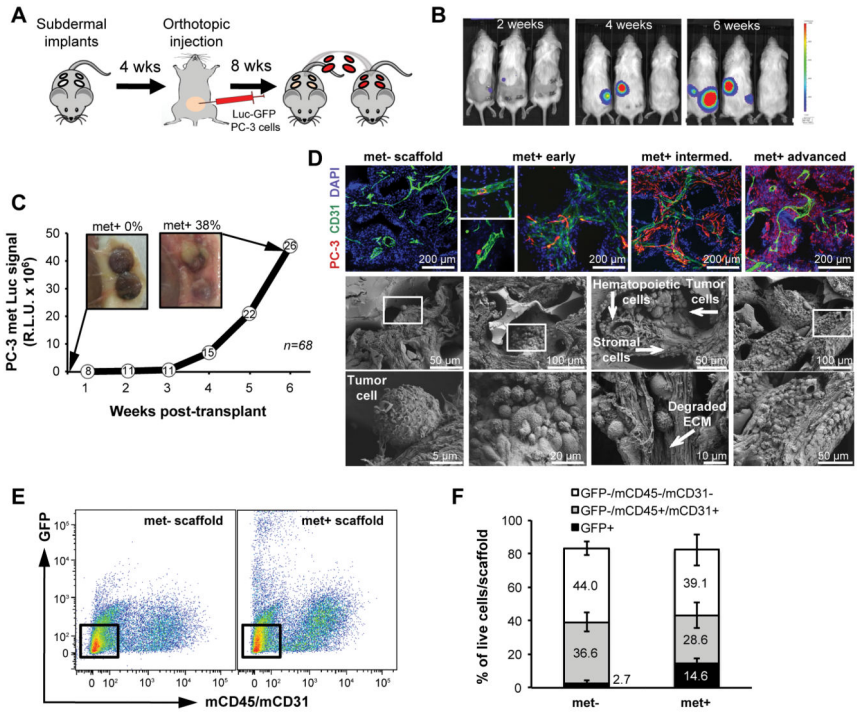

Figure 3.

Serial transplantation of scaffolds into naïve mice enables tracking of metastatic progression in scaffold microenvironments. A, scaffolds from primary orthotopic prostate tumor-bearing mice were transplanted into tumor-free syngeneic mice for long-term monitoring of metastatic progression. B, representative BLI images after serial transplant showing metastatic growth in the scaffolds. C, increased BLI signal from met+ scaffolds with gross images before and after serial transplant. Values are expressed as the R.L.U. (relative luciferase unit) sum of all positive scaffolds at any given time (number of met+ scaffolds indicated in the white circles; *n*=68). D, representative images of metastatic progression shown by immunofluorescence (top; blue=DAPI, green=mCD31, red=hVimentin) and SEM images of scaffold microenvironments (bottom). The scaffold pore composition includes hematopoietic, stromal and tumor cells with evidence of tumor/stromal interaction and local ECM degradation. Boxed areas in the middle panels are magnified in the lower panels. E, fluorescence activated cell sorting of cells recovered from met− and met+ PC-3 scaffolds. Boxed areas show stromal cells (GFP−/mCD45−/mCD31−). F, comparison of the relative cellular composition of met− vs met+ scaffolds from the PC-3 model by flow cytometry using the indicated antibodies. Bars represent SD (*n*=3).

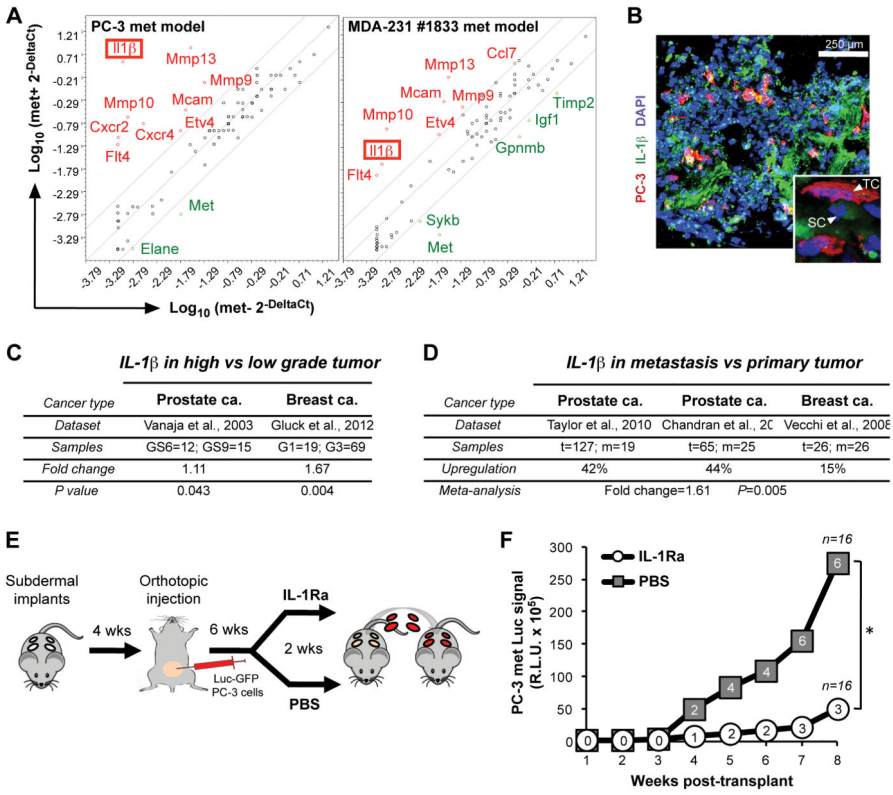

Figure 4.

Profiling of scaffold microenvironments leads to the identification of IL-1β as a key component of the metastatic stromal compartment. A, comparison of gene expression profiles of stromal cells retrieved from met+ (PC-3, *n*=2; MDA-231, *n*=5) vs met− (*n*=3) scaffolds of the indicated tumor cell metastasis models. Since no uninvolved scaffolds were available for the breast cancer model, met− scaffolds obtained from PC-3 mice were used as their negative control. Red and green indicate up- and down-regulated genes in met+ scaffolds, respectively. B, immunofluorescence staining of IL-1β (both mouse- and human-specific) in met+ scaffolds. Inset shows a high magnification field (TC=tumor cell; SC=stromal cell). C, IL-1β expression correlation with primary tumor Gleason score (GS) or grade (G) in a prostate and a breast cancer dataset, respectively. D, meta-analysis of IL-1β across available prostate and breast cancer datasets (t=primary tumor; m=metastasis). E, experimental design to test the therapeutic effect of IL-1β neutralization on metastasis formation. F, longitudinal monitoring of overall BLI signal, expressed as the R.L.U. (relative luciferase unit) sum of all positive scaffolds at any given time, of IL-1Ra- and PBS-treated mice after serial transplant. The number of met+ scaffolds is indicated in white circles and grey squares for IL-1Ra and PBS treatment respectively (*n*=16; **P*<0.005).